Journal of Material Cycles and Waste Management (2020) 22:1208–1217
https://doi.org/10.1007/s10163-020-01015-4

ORIGINAL ARTICLE

# Effect of $B_2O_3$ addition on mineralogical phases and leaching behavior of synthetic CaO–$SiO_2$–MgO–$Al_2O_3$–$CrO_x$ slag

Yong Lin[1] · Qingyun Luo[1] · Baijun Yan[1] · Timo Fabritius[2] · Qifeng Shu[1,2]

Received: 5 November 2019 / Accepted: 6 March 2020 / Published online: 18 March 2020


## Abstract

Boron oxide is frequently applied in modification of stainless steelmaking slag to mitigate the disintegration of slag. In this work, the effect of $B_2O_3$ on mineralogical phases and hexavalent chromium leaching behavior of synthetic CaO–$SiO_2$–MgO–$Al_2O_3$–$CrO_x$ slag was investigated. Di-calcium silicate, merwinite, spinel, akermanite, and matrix phase were observed as main minerals in slags by scanning electron microscope (SEM) equipped with energy-dispersive spectrometry (EDS) and X-ray diffraction (XRD) techniques. It was found that 2% $B_2O_3$ addition is sufficient to eliminate the disintegration of synthetic slag by suppressing the phase transition to $\gamma$-$Ca_2SiO_4$. The size of spinel phase increases with increasing $B_2O_3$, which could be well interpreted by enhanced Ostwald ripening. The amount of $Ca_2SiO_4$ phase in slag was reduced by addition of $B_2O_3$; however, excess $B_2O_3$ (> 2%) addition would significantly increase chromium concentration and overall chromium distribution in $Ca_2SiO_4$ phase. Leaching results according to US-EPA-3060A method indicated that excess boron oxide addition (> 2%) leads to a significant increase of hexavalent chromium leaching concentrations and should be avoided for stabilizing stainless steel slag.

**Keywords** Boron oxide · Stainless steel slag · Chromium · Mineralogical phase · Leaching behavior

## Introduction

Stainless steel slag is generated in the production of stainless steel. Generally, stainless steel slag consists of CaO, $SiO_2$, MgO, and some amount of $Cr_2O_3$ (< 10%) that originates from the oxidation of chromium during alloying process. The valence state of chromium in stainless steel slag is mainly divalent ($Cr^{2+}$) or trivalent ($Cr^{3+}$) that has low toxicity. Unfortunately, low valent chromium could be oxidized into highly toxic hexavalent chromium ($Cr^{6+}$) when exposed to acidic and oxygen-rich environments [1]. Hexavalent chromium is water-soluble and easy to be leached into underground water to produce serious environmental pollution. Moreover, disintegration behavior is commonly observed in stainless steel slag during natural cooling [2], which is generally caused by the phase transition from $\beta$-$Ca_2SiO_4$ to $\gamma$-$Ca_2SiO_4$ accompanied by 12% volume expansion [3]. The leaching of hazardous hexavalent chromium could also be aggravated by the disintegration behavior. Therefore, the utilization of stainless steel slag is still limited.

To suppress the disintegration behavior and immobilize the chromium in slag, many stabilization techniques for slag have been proposed. The mitigation of disintegration of slag could be achieved by some physical methods, such as rapid cooling to suppress the phase transition [3]. The modification of slag could be performed by additives to mitigate the disintegration of slag and immobilize chromium in slag [4–9]. It is well accepted that spinel phase is very stable during oxidation and leaching due to the strong bonding of chromium in spinel phase [2]. Modification with MgO could mitigate the precipitation of $Ca_2SiO_4$ [4] and be beneficial to spinel formation during solidification of slag [5, 6]. The additions of appropriate amounts of $Al_2O_3$ [5, 7], MnO [8], and FeO [9] were found to promote the spinel formation. Meanwhile, low basicity [6, 8, 10] and oxygen partial pressure [11] have a positive influence on spinel precipitation.

Boron oxide has been found to be an excellent stabilizer for stainless steel slag [12–16]. Ghose et al. concluded that

✉ Qifeng Shu
shuqifeng@gmail.com; qifeng.shu@oulu.fi

[1] School of Metallurgical and Ecological Engineering, University of Science and Technology Beijing, Beijing 100083, China

[2] Research Unit of Process Metallurgy, University of Oulu, 90014 Oulu, Finland

0.13 wt% $B_2O_3$ can already stabilize the $\beta$-polymorph of $Ca_2SiO_4$ [12]. Seki et al. developed a borate-based stabilizer for stainless steel decarburisation slag [13]. Durinck et al. considered that the crystallographic mechanism could be the partial replacement of $SiO_4^{4-}$ units by $BO_3^{3-}$ units that suppresses the $Ca^{2+}$ migrations and $SiO_4^{4-}$ rotations required for the $\beta$-$Ca_2SiO_4$ to $\gamma$-$Ca_2SiO_4$ transformation [14]. Wu et al. studied the influence of $B_2O_3$ on crystallization behavior of Cr-bearing phase in stainless steel slag [15]. They found that the size of Cr-bearing phase in slag with $B_2O_3$ enhanced as an increase of holding time and the content of $Cr_2O_3$ in the spinel phase was higher than that in the slag without $B_2O_3$ [15]. Based on the fact that boron can stabilize stainless steel slag effectively, boron-contained materials have been applied for the stabilization of stainless steel slag in some steel companies [13, 16]. The boron-contained materials are usually added into molten stainless steel slag during the slag discharge process. However, the effect of boron oxide addition on leaching behavior of hexavalent chromium in treated stainless steel slag received only a few investigations. Recently, Li and Xue investigated the effect of boron oxide addition on the chromium distribution in Cr-bearing phase and emission of hexavalent chromium [17]. They reported that the leachability of hexavalent chromium was enhanced with increasing of boron oxide content in some cases [17]. Unfortunately, the detailed mechanism for that was not discussed in their work. Accordingly, the effects of $B_2O_3$ on mineralogical phases and chromium leaching of slags still require further studies.

In the present work, the effect of $B_2O_3$ addition on the phase formations in synthetic CaO–$SiO_2$–MgO–$Al_2O_3$–$CrO_x$ slag was investigated under a low oxygen partial pressure ($P_{O2} = 10^{-10}$ atm). The chromium distributions in different mineralogical phases were quantified. Furthermore, the leaching concentrations of hexavalent chromium were also evaluated according to US-EPA-3060A method [18].

## Materials and methods

Reagent-grade compounds CaO, $SiO_2$, $Al_2O_3$, MgO, $Cr_2O_3$, and $H_3BO_3$ were taken as raw materials. The chemical compositions of the samples investigated are listed in Table 1. Reagent-grade $CaCO_3$ was calcined at 1373 K overnight in muffle furnace to obtain CaO. To avoid the occurrence of hydroxide and carbonate, MgO was also calcined at 1273 K for 6 h in muffle furnace. $SiO_2$, $Al_2O_3$, and $Cr_2O_3$ were dried at 393 K for 4 h in an oven to remove moistures. $H_3BO_3$ as a substitute of $B_2O_3$ was added directly without drying in the present work for the reason of its low melting point (449 K) [19]. The basicity of synthetic slag (defined as the mass ratio of CaO to $SiO_2$) was maintained as 1.5, considering that the basicity of industrial stainless steel slag is generally in the range of 1.0 ~ 2.5 [5–11]. The contents of MgO, $Al_2O_3$, and $Cr_2O_3$ in slags were fixed as 8.0, 6.0, and 6.0, respectively. The reagent powders were mixed with appropriate ratios and pressed into pellets. The pellets were loaded in molybdenum crucibles, and then located in the even temperature zone of a tube furnace with molybdenum silicide as heating elements using molybdenum wire. Schematic diagram of the furnace can be found in our previous publication [20]. A W-Re5/26 thermocouple was installed underneath the bottom of molybdenum crucible to measure and control the temperature within the furnace. Oxygen partial pressure of $10^{-10}$ atm was maintained by mixing gas of CO and $CO_2$ ($CO/CO_2 = 41$). The flow rate of gases was controlled by two mass flow meters (Bronkhorst EL-FLOW Base). Samples were heated to 1873 K slowly followed by cooling to room temperature with a rate of 5 K·min$^{-1}$.

After cooling, the mineralogical phases in samples were investigated using scanning electron microscopy equipped with energy-dispersive spectra (SEM–EDS) and X-ray diffraction (XRD). For SEM examination, samples were embedded with epoxy resin and prepared by standard metallographic preparation methods. The SEM examination was performed on FEI MLA 250. The working voltage was 20 kV.

The XRD spectra were collected with an 18 kW X-ray diffractometer (model: Rigaku TTR III, Japan) with Cu–K$\alpha$ radiation. The 2θ scanning range was 15°–65° with a scan speed of 2 s step$^{-1}$. The mass percentages of various crystalline phases were determined using an X-ray quantitative analysis method based on RIR (Relative Intensity Ratio) values [21], which was described briefly as follows.

The ratio of mass percentage of $\alpha$ phase to $\beta$ phase could be calculated from intensities of the strongest peaks for $\alpha$ phase to $\beta$ phase according to the following equation:

**Table 1** Chemical compositions of samples investigated in the present work (wt%)

| Sample No | CaO | $SiO_2$ | MgO | $Al_2O_3$ | $Cr_2O_3$ | $B_2O_3$ | Basicity |
|---|---|---|---|---|---|---|---|
| 1 | 48.0 | 32.0 | 8.0 | 6.0 | 6.0 | 0 | 1.5 |
| 2 | 46.8 | 31.2 | 8.0 | 6.0 | 6.0 | 2 | 1.5 |
| 3 | 45.6 | 30.4 | 8.0 | 6.0 | 6.0 | 4 | 1.5 |
| 4 | 44.4 | 29.6 | 8.0 | 6.0 | 6.0 | 6 | 1.5 |

$$\frac{\omega(\alpha)}{\omega(\beta)} = \frac{I(\alpha)/\mathrm{RIR}(\alpha)}{I(\beta)/\mathrm{RIR}(\beta)}, \quad (1)$$

where $\omega(\alpha)$ and $\omega(\beta)$ are mass percentages of $\alpha$ and $\beta$ phases, respectively. RIR($\alpha$) and RIR($\beta$) are relative intensity ratio values for $\alpha$ and $\beta$ phases, respectively. I($\alpha$) and I($\beta$) are intensities of the strongest peaks for $\alpha$ and $\beta$ phases, respectively. RIR values for various phase could be found in Joint Committee on Powder Diffraction Standards-International Centre for Diffraction Data (JCPDS-ICDD) cards. Thus, mass percentages of various phases could be calculated using intensities of the strongest peaks and RIR values for various phases.

US-EPA-3060A method, an alkaline digestion step, is widely used to assess the leaching concentration of hexavalent chromium in solid waste [18]. According to the standard procedure, the alkaline digestion was carried out on 2.5 g samples in this work. The leaching agent was 50 mL alkaline solution containing 0.28 M $Na_2CO_3$ and 0.5 M NaOH. 400 mg anhydrous $MgCl_2$ and 0.5 mL buffer solution (0.5 M $K_2HPO_4$ and 0.5 M $KH_2PO_4$) were also added into the beaker to avoid oxidation of trivalent chromium. After digesting, the suspensions were filtered by vacuum filtration process with a 0.45 μm standard filter paper. Subsequently, the chromium concentration in filtrate was detected by inductively coupled plasma-optical emission spectrometer (ICP-OES, Optima-7000DV, Perkin Elmer).

The mineralogical phases of slags determined by SEM–EDS and XRD techniques were also compared with the simulation results calculated by a commercial thermodynamic software, FactSage 7.0 (Thermfact and GTT-technologies) [22]. FToxide database and Scheil–Gulliver cooling model [23] were employed during calculation.

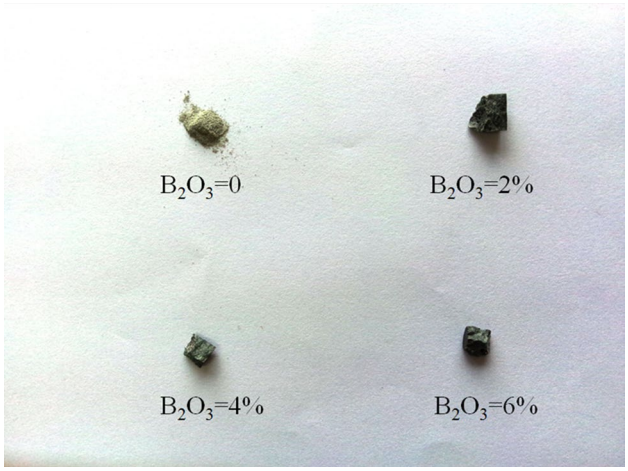


**Fig. 1** Morphology of samples containing different $B_2O_3$ contents

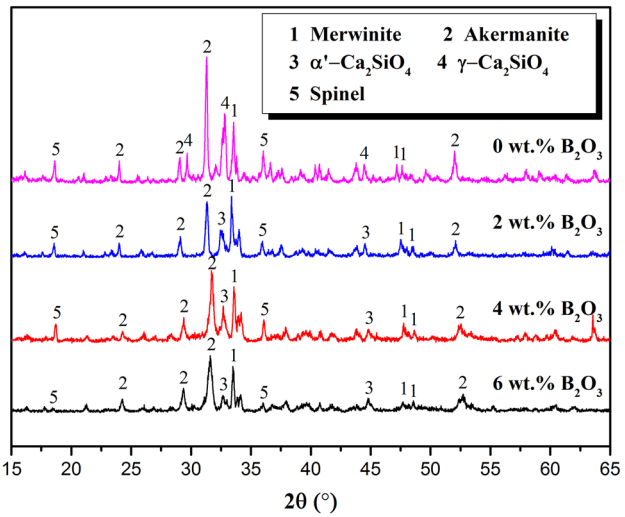


**Fig. 2** XRD patterns for samples with different amount of $B_2O_3$ addition

## Results and discussion

### Disintegration behavior of slags

Figure 1 shows the morphology of samples containing different $B_2O_3$ contents after cooling. The sample free of $B_2O_3$ showed very serious disintegration behavior, while other samples showed no disintegration. This indicates that only slight addition of 2% $B_2O_3$ would mitigate the disintegration of slag. It is well known that di-calcium silicate exists in five different polymorphic forms: α, $\alpha'_H$, $\alpha'_L$, β, and γ [24]. $\alpha$-$Ca_2SiO_4$ is stable at high temperature and $\gamma$-$Ca_2SiO_4$ is stable at room temperature. $\alpha'$-$Ca_2SiO_4$ has two different forms, $\alpha'_H$-$Ca_2SiO_4$ and $\alpha'_L$-$Ca_2SiO_4$, originating from the translocation of calcium atoms. $\beta$-$Ca_2SiO_4$ is a kind of metastable substance, which usually transforms to $\gamma$-$Ca_2SiO_4$ at 673–773 K during slow cooling. Due to the difference of density between them ($\rho(\beta\text{-}Ca_2SiO_4) = 3.28\ g{\cdot}cm^{-1}$, $\rho(\gamma\text{-}Ca_2SiO_4) = 2.97\ g{\cdot}cm^{-1}$) [13], the phase transition is accompanied by 12% volume expansion, which is attributed to be the main reason for slag disintegration [3]. The XRD patterns for various samples are presented in Fig. 2. $\gamma$-$Ca_2SiO_4$ which is the stable form of $Ca_2SiO_4$ at room temperature can be found in the slag free of $B_2O_3$, indicating that the sample underwent phase transition during slow cooling. By comparison, high-temperature form $\alpha'$-$Ca_2SiO_4$ dominantly existed in the samples with addition of $B_2O_3$. Therefore, addition of $B_2O_3$ can effectively suppress the phase transition of $Ca_2SiO_4$ and mitigate the disintegration behavior of stainless steel slag.

## Mineralogical phases in slags

Mineralogical phases in all samples were determined by combining XRD with SEM–EDS analysis, as presented in Figs. 2 and 3, respectively. Four crystalline phases as $Ca_2SiO_4$ in light gray, merwinite in dark gray, akermanite in light black, and spinel in white were identified in SEM micrographs by EDS. Determined average chemical compositions of various phases are summarized in Table 2. The concentration of matrix in sample free of boron oxide was not determined due to its disintegration nature. The XRD patterns of samples also showed the existence of four kinds of crystalline phases. The mass percentages of crystalline phases in samples were determined by X-ray quantitative analysis and are presented in Table 3. It should be mentioned that the mass percentage of matrix cannot be determined by the method employed and it is excluded in the calculation of mass percentage of crystalline phases. It could be found from the micrographs of various samples that the matrix phases actually are very few due to the strong crystallization during cooling.

The phase precipitations of various slags during cooling were simulated by FactSage using Scheil–Gulliver model. The results are shown in Fig. 4. Spinel is the first crystalline phase during slag cooling, followed by $Ca_2SiO_4$, merwinite, and akermanite for the slags with $B_2O_3\% = 0$, 2, and 4%, which is in consistence with experimental results. For the slag with $B_2O_3\% = 6\%$, FactSage calculation predicts that there is no precipitation of $Ca_2SiO_4$ which is contradict to the experimental results. This could be due

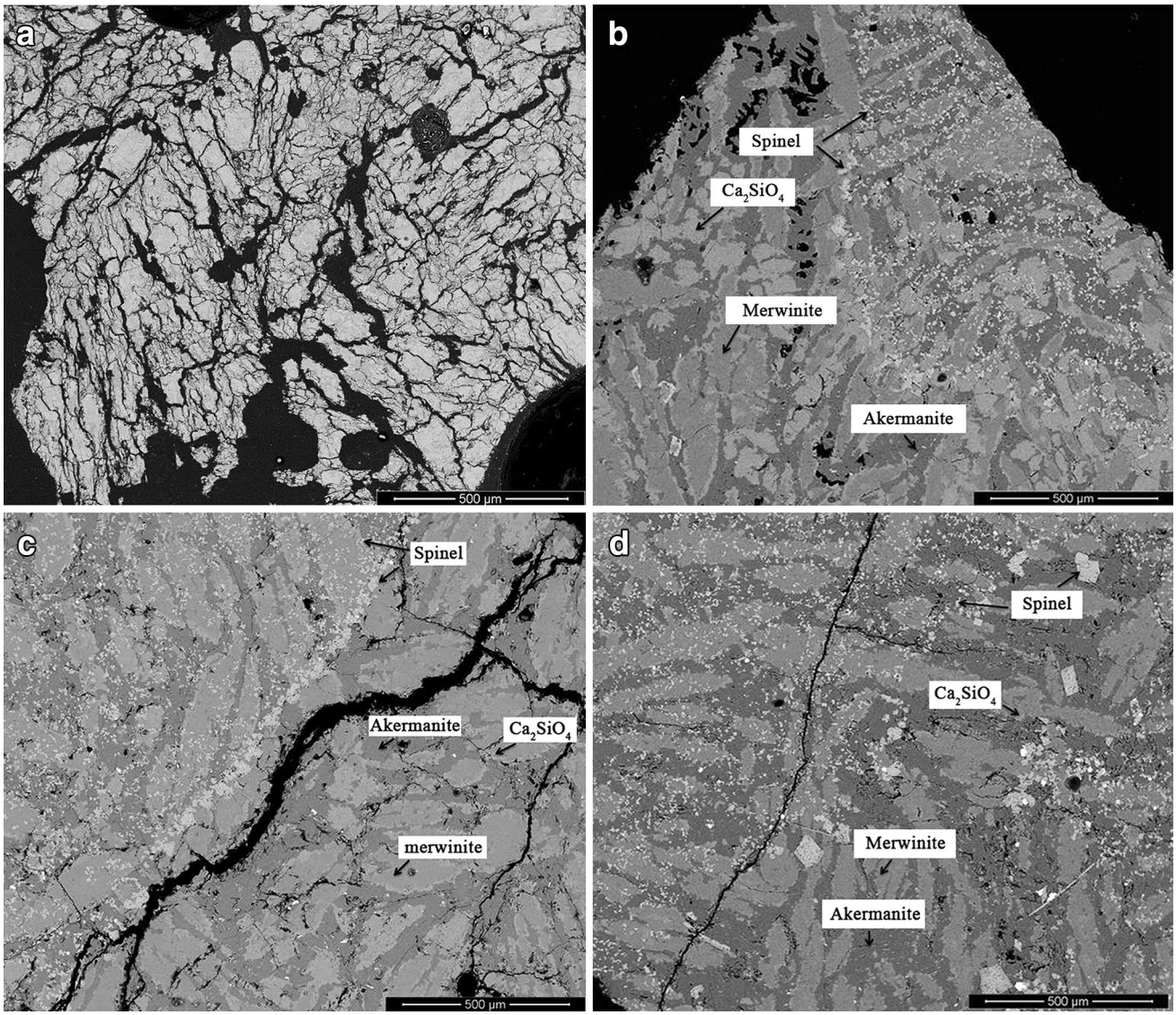


**Fig. 3** SEM images of the samples with different amount of $B_2O_3$ addition: **a** $0\%B_2O_3$, **b** $2\%B_2O_3$, **c** $4\%B_2O_3$, and **d** $6\%B_2O_3$

**Table 2** Averaged chemical compositions (wt%) of various mineralogical phases determined by EDS and calculated $Cr_2O_3$ distribution in each phase (%)

| Sample | $B_2O_3$% | Phase | CaO | $SiO_2$ | MgO | $Al_2O_3$ | $Cr_2O_3$ | $B_2O_3$ | $Cr_2O_3$ distribution |
|---|---|---|---|---|---|---|---|---|---|
| 1 | 0 | Spinel | 4.28 | 2.20 | 15.65 | 13.29 | 65.48 | – | 3.62 |
| | | $Ca_2SiO_4$ | 65.11 | 26.89 | 5.26 | 2.01 | 0.73 | – | 0.25 |
| | | Merwinite | 61.00 | 28.67 | 10.33 | 0 | 0 | – | 0 |
| | | Akermanite | 52.19 | 28.75 | 8.01 | 11.06 | 0 | – | 0 |
| 2 | 2 | Spinel | 2.30 | 0.77 | 24.26 | 17.05 | 54.56 | 1.07 | 2.44 |
| | | $Ca_2SiO_4$ | 54.35 | 35.12 | 5.33 | 0.16 | 0.79 | 4.25 | 0.19 |
| | | Merwinite | 50.20 | 37.31 | 11.95 | 0.15 | 0.38 | 0 | 0.18 |
| | | Akermanite | 39.58 | 33.52 | 5.63 | 19.79 | 0.12 | 1.36 | 0.03 |
| | | Matrix | 37.61 | 33.09 | 6.09 | 19.15 | 0.09 | 3.97 | – |
| 3 | 4 | Spinel | 0.23 | 0.03 | 22.45 | 12.99 | 64.14 | 0.16 | 2.01 |
| | | $Ca_2SiO_4$ | 52.50 | 28.04 | 2.57 | 0.50 | 4.40 | 11.98 | 1.02 |
| | | Merwinite | 47.65 | 34.52 | 10.85 | 0.13 | 1.09 | 5.77 | 0.49 |
| | | Akermanite | 37.75 | 31.63 | 6.17 | 15.59 | 0.23 | 8.63 | 0.07 |
| | | Matrix | 45.17 | 15.36 | 3.68 | 1.50 | 0.37 | 33.91 | – |
| 4 | 6 | Spinel | 1.08 | 0.08 | 22.76 | 8.69 | 67.40 | 0 | 2.15 |
| | | $Ca_2SiO_4$ | 53.24 | 29.45 | 2.82 | 1.66 | 2.99 | 9.84 | 0.61 |
| | | Merwinite | 47.87 | 33.24 | 11.66 | 0.13 | 0.95 | 6.15 | 0.42 |
| | | Akermanite | 36.39 | 25.69 | 3.93 | 9.44 | 0.50 | 24.05 | 0.16 |
| | | Matrix | 42.79 | 16.17 | 1.40 | 3.12 | 1.04 | 35.47 | – |

**Table 3** Mass percentage of various crystalline phases in samples determined by XRD (%)

| Mineralogical phases | Sample 1 (0% $B_2O_3$) | Sample 2 (2% $B_2O_3$) | Sample 3 (4% $B_2O_3$) | Sample 4 (6% $B_2O_3$) |
|---|---|---|---|---|
| Spinel | 5.53 | 4.47 | 3.14 | 3.19 |
| $Ca_2SiO_4$ | 33.72 | 24.81 | 23.30 | 20.42 |
| Merwinite | 26.07 | 46.58 | 45.17 | 44.73 |
| Akermanite | 34.68 | 24.14 | 28.39 | 31.65 |

to the kinetic factor involved in the crystallization of slags. There are some existence of spinel and $Ca_2SiO_4$ at 1873 K in FactSage calculation results, indicating that the synthetic slag should be solid–liquid coexisting slag at high temperature. The proportion of liquid phase in $B_2O_3$-free sample was about 55% at 1873 K, and increased continuously up to 95% after adding $B_2O_3$, indicating that $B_2O_3$ is beneficial to melting of slag. Some slight increase of spinel mass was found during cooling in calculation results, indicating slight precipitation of spinel during cooling. The total precipitation amount of spinel was maintained unchanged at 10% with addition of $B_2O_3$. In contrast to the experimental results, $Ca_3Si_2O_7$ and $CaSiO_3$ were found to be precipitated at low temperature for samples with 4 and 6% $B_2O_3$ addition in FactSage calculation. This inconsistency could be also due to the kinetic factors for crystallization. The calculated amount of precipitated $Ca_2SiO_4$ decreased with increasing $B_2O_3$ content for the slags with $B_2O_3$% = 0, 2, and 4%.

As seen in Fig. 2, the intensity of characteristic diffraction peak of $Ca_2SiO_4$ at $2\theta = 32.6°$ was reduced obviously with increasing $B_2O_3$ content in slag. The mass percentage of $Ca_2SiO_4$ determined by XRD quantitative analysis (see Table 3) decreased from 33.72 to 20.42% as $B_2O_3$ content increases from 0 to 6%. The FactSage simulation results shown in Fig. 4 also indicate that the precipitated amount of $Ca_2SiO_4$ decreases as $B_2O_3$ increases from 0 to 4%. Therefore, the addition of $B_2O_3$ would suppress the crystallization of $Ca_2SiO_4$. However, the concentrations of chromium in $Ca_2SiO_4$ phase were found to be significantly increased with addition of $B_2O_3$. As listed in Table 2, in samples free of $B_2O_3$ and with 2% $B_2O_3$, there were only slight $Cr_2O_3$ content (0.73%, 0.79%) in $Ca_2SiO_4$ phase. While for samples with 4 and 6% $B_2O_3$ addition, 4.40 and 2.99% $Cr_2O_3$ were found to be in $Ca_2SiO_4$ phase, respectively. The overall amount of $Cr_2O_3$ distributed in each phase can be calculated by multiplying the mass percentage of each phase by the concentration of $Cr_2O_3$ in each phase. The calculated $Cr_2O_3$ distributions in various phases are also listed in Table 2. It could be seen that spinel phase has the largest $Cr_2O_3$ distribution, followed by di-calcium silicate phase. As shown in Fig. 5, although the mass percentage of di-calcium silicate phase decreases all the time, the $Cr_2O_3$ distribution in di-calcium silicate phase is significantly enhanced by excess addition (> 2%) of $B_2O_3$. In samples with $B_2O_3$% = 0 and 2%,

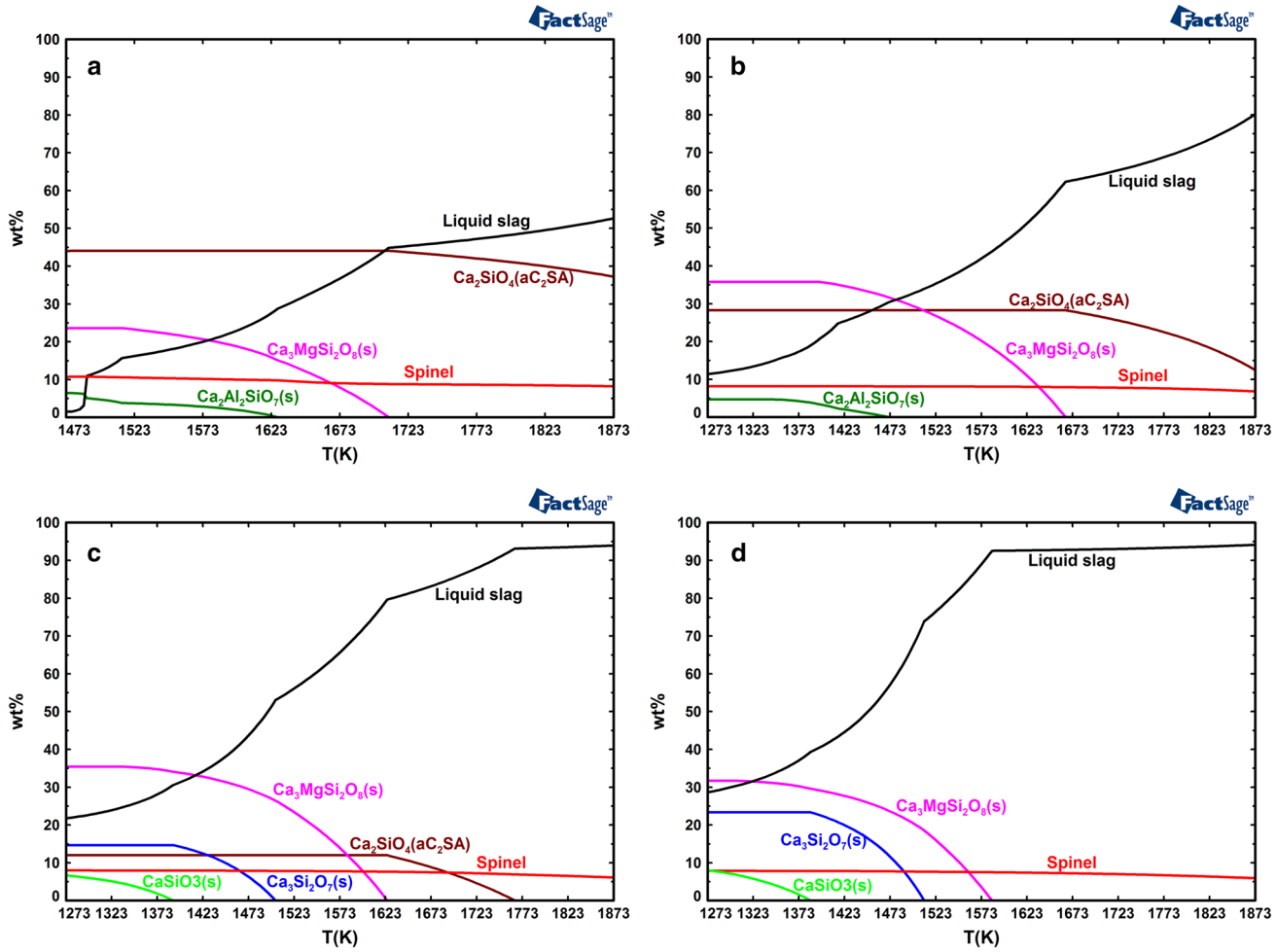


**Fig. 4** FactSage simulation results on phase precipitation using Scheil-Gulliver model

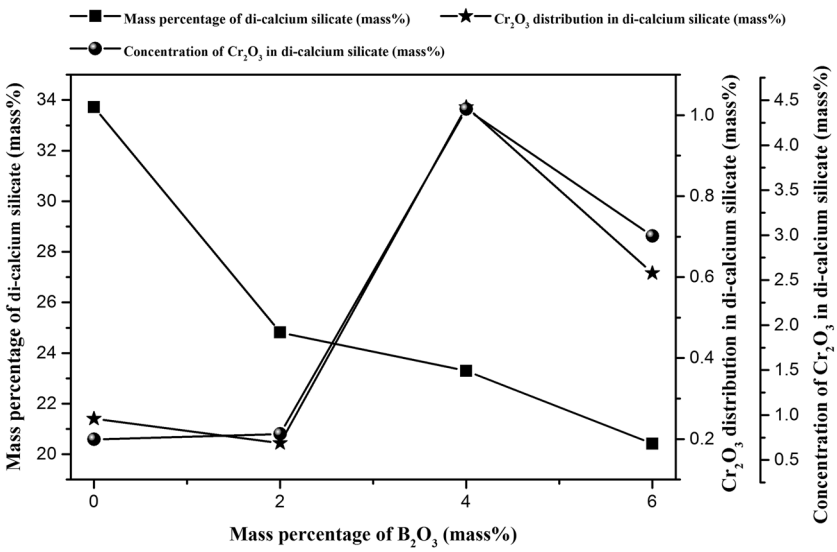


**Fig. 5** Mass percentage of $Ca_2SiO_4$, content of $Cr_2O_3$ in $Ca_2SiO_4$ and $Cr_2O_3$ distribution as function of content of $B_2O_3$

the $Cr_2O_3$ distributions (0.25%, 0.19%) in di-calcium silicate phase are much lower than those in spinel phase (3.62%, 2.44%). With further $B_2O_3$ addition, the $Cr_2O_3$ distribution in di-calcium silicate phase significantly increases. In samples with $B_2O_3$% = 4 and 6%, the $Cr_2O_3$ distributions (1.02%, 0.61%) in di-calcium silicate phase could be compared with those (2.01%, 2.15%) in spinel phase. The overall amount of $Cr_2O_3$ distributed in di-calcium silicate phase is significantly increased for samples with excess $B_2O_3$ addition due to the large increase of the concentrations of chromium in $Ca_2SiO_4$ phase.

Generally, chromium has several valence states such as $Cr^{2+}$, $Cr^{3+}$, and $Cr^{6+}$. Many factors such as composition, melting temperature, and oxygen partial pressure have some influences on the valence of chromium in slags. Pretorious [25] and Wang [26] concluded that divalent chromium predominates in the high-temperature system with low oxygen partial pressure and basicity. Due to the fact that all the samples were heated to 1873 K in low oxygen partial pressure atmosphere ($10^{-10}$ atm), the predominant valance state of chromium in the slag samples was $Cr^{2+}$. Villiers et al. studied the liquidus–solidus phase relations in the system of CaO–CrO–$Cr_2O_3$–$SiO_2$ [27]. They found that there is considerable solid solution of chromium oxide in lime and various crystalline calcium silicates (pseudowollastonite, $CaSiO_3$; rankinite, $Ca_3Si_2O_7$; di-calcium silicate, $Ca_2SiO_4$; tricalcium silicate, $Ca_3SiO_5$), particularly in lime and $Ca_2SiO_4$, the reason of which was that $Cr^{2+}$ partially substituted $Ca^{2+}$ sites. Moreover, Cuesta et al. investigated the solid solution mechanisms of B in $Ca_2SiO_4$ by testing three nominal solid solution ($Ca_{2-x/2}\square_{x/2}(SiO_4)_{1-x}(BO_3)_x$; $Ca_2(SiO_4)_{1-x}(BO_3)_xO_{x/2}$; $Ca_{2-x}B_x(SiO_4)_{1-x}(BO_4)_x$) [28]. They proposed that boron stabilizes $Ca_2SiO_4$ by substituting jointly silicon unites as $BO_4^{5-}$ and calcium cations by $B^{3+}$. Therefore, increasing the content of $B_2O_3$ in samples would lead to more replacement of $SiO_4^{4-}$ by $BO_4^{5-}$ in $Ca_2SiO_4$ phase. The $BO_4^{5-}$ is charge deficient compared with $SiO_4^{4-}$; the charge compensation is required to stabilize the structure of di-calcium silicate [29]. As cations for charge compensation, more $Cr^{2+}$ ions would dissolve into $Ca_2SiO_4$ phase to maintain the electro-neutrality.

As shown in Fig. 3, the size of spinel phase in slag is enlarged with $B_2O_3$ addition. According to the XRD quantification results in Table 3 and FactSage simulation results in Fig. 4, the mass of spinel phase in slag only slightly changes during cooling. Accordingly, the spinel phase mainly undergoes coarsening during cooling. As shown in Fig. 3, the size increases for spinel phase with addition of $B_2O_3$, and some spinel particles with extra large size (larger than 100 μm) could be found. This might be explained by Ostwald ripening that is known as a process in which large crystals grow with time at the expense of the small ones in a system consisting of crystals and liquids [30, 31]. The classical Lifshitz–Slyozov–Wagner (LSW) theory predicts the ripening kinetics very well; the equation is as follows [31]:

$$\bar{d}^3 - \bar{d}_0^3 = \frac{64D\sigma_{SL}V_S c_o}{9RT}t, \tag{2}$$

where $\bar{d}$ is the mean crystal size at time $t$; $\bar{d}_0$ is the initial mean crystal size; $D$ is effective diffusion coefficient; $\sigma_{SL}$ is solid–liquid interfacial tension; $V_S$ is the molar volume of crystal; $c_0$ is the mass concentration of mobile species in liquid equilibrated with a crystal with infinite large size. The effective diffusion coefficient has a relationship with viscosity according to the well-known Stokes–Einstein equation [32]:

$$D = \frac{kT}{6\pi r\eta}, \tag{3}$$

where $D$ is diffusion coefficient of ions in slag; $\eta$ is viscosity of slag; $T$ is temperature in Kelvin; $k$ is Boltzmann constant; r is radius of ions in slag. It could be seen from Eqs. (2) and (3) that the viscosity of slag plays a dominant role in coarsening of crystals in slag. Li et al. reported that $B_2O_3$ addition leads to the formation of low melting point eutectics and weaker polymerization strength, which contribute to the decrease in slag viscosity [33]. Therefore, according to Eqs. (2) and (3), the ripening rate would be promoted with addition of $B_2O_3$, and larger size of spinel phase could be found in samples with more $B_2O_3$ addition.

## Leaching concentration of hexavalent chromium in slags

The leaching concentrations of hexavalent chromium in all samples were determined using US-EPA-3060A method and are shown in Fig. 6. Leaching concentration value of

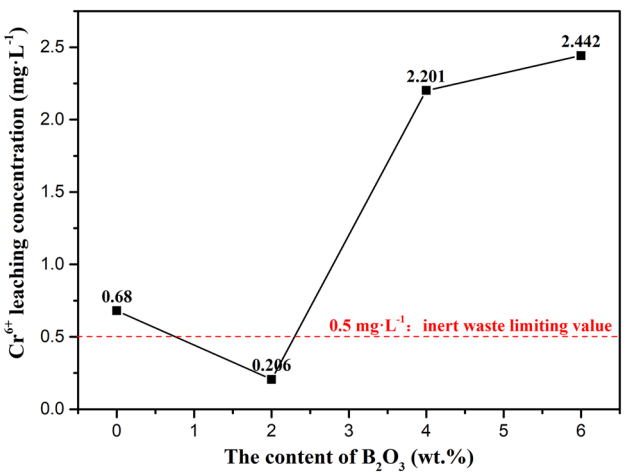


**Fig. 6** Chromium leaching concentrations of synthetic slag samples

0.68 mg·$L^{-1}$ for hexavalent chromium was detected for the sample free of $B_2O_3$, which exceeded the inert waste limiting value (0.5 mg·$L^{-1}$ [34]). The addition of 2% $B_2O_3$ reduced the leaching concentration value to 0.206 mg·$L^{-1}$. However, the hexavalent chromium concentrations increased rapidly with further addition of $B_2O_3$. Leaching concentration values of 2.201 and 2.442 mg·$L^{-1}$ for hexavalent chromium were detected in the leaching solutions of samples with $B_2O_3 = 4\%$ and 6%, respectively. Such high concentrations of hexavalent chromium demonstrated that the stainless steel slags with excess $B_2O_3$ addition (> 2%) were unstable for leaching of hexavalent chromium.

The effect of $B_2O_3$ addition on leaching behavior of synthetic slag could be interpreted by considering the variation of mineralogical phases in slag. Mineralogical phases of $Ca_2SiO_4$, merwinite, akermanite, and spinel were confirmed to be main minerals in slag samples. It is generally accepted that chromium in spinel phase is hardly to be leached out due to its incorporation into spinel structure [2]. Engström et al. investigated the dissolution of merwinite, akermanite, and $\gamma$-$Ca_2SiO_4$ using $HNO_3$ solution at constant pH, and concluded that the dissolution rates for merwinite and akermanite phase are pH-dependent [35]. When the pH value is higher than 10, dissolution of merwinite and akermanite is considered negligible. The dissolution of $\gamma$-$Ca_2SiO_4$ is not affected in the same way as merwinite and akermanite when the pH is changed [35]. They also reported that boron-stabilized $\beta$-$Ca_2SiO_4$ was the only mineral fully dissolved at pH 4, 7 and 10 [36]. Moreover, Teratoko et al. investigated the dissolution behavior of di-calcium silicate in an aqueous solution, and found that the solubility of $Ca_2SiO_4$ was much greater than other phases of steelmaking slag [37]. Samada et al. concluded that the existence of $Ca_2SiO_4$ enhanced the dissolution of chromium into seawater [38]. At the present work, the leaching agent was 50 mL alkaline solution containing 0.28 M $Na_2CO_3$ and 0.5 M NaOH, the pH value of which was 11.5 or greater [18]. Therefore, it can be inferred that $Ca_2SiO_4$ is a kind of easy dissolution mineral in slag and could be dissolved at pH = 11.5, while merwinite, akermanite, and spinel phase could not be easily dissolved. The main contribution to the leaching of hexavalent chromium should be $Ca_2SiO_4$. According to Table 2, the chromium distributions in $Ca_2SiO_4$ for samples with $B_2O_3 = 4\%$ and 6% were significantly higher than those in samples with $B_2O_3 = 0$ and 2%. This could be the main reason for the higher leaching concentration of the hexavalent chromium for samples with $B_2O_3 = 4\%$ and 6%. It can be noticed that the $Cr_2O_3$ distribution in $Ca_2SiO_4$ for sample with $B_2O_3 = 6\%$ is lower than that of sample with $B_2O_3 = 4\%$, while the leaching of hexavalent chromium in sample with $B_2O_3 = 6\%$ is still higher than that of sample with $B_2O_3 = 4\%$. This could be due to the dissolution of Cr in matrix phase of sample with $B_2O_3 = 6\%$. As seen in Table 2, the Cr concentration in matrix phase for sample with $B_2O_3 = 6\%$ is much higher than other samples.

In summary, the size of spinel phase increased with increasing $B_2O_3$ content in slags and majority of chromium were found enriched in spinel phase. Whereas the chromium concentration in $Ca_2SiO_4$ phase was also enhanced, leading to increasing the leaching concentration of hexavalent chromium. Therefore, the addition content of boron-contained materials must be controlled in practical application. We concluded that excess boron oxide content (> 2%) should be avoided for stabilizing stainless steel slag.

## Conclusions

The effect of $B_2O_3$ on mineralogical phases and leaching behavior in synthetic CaO–$SiO_2$–MgO–$Al_2O_3$–$CrO_x$ slag was investigated under the condition of low oxygen partial pressure ($P_{O2} = 10^{-10}$ atm). SEM–EDS and XRD were employed to determine the phase composition. The simulations on phase precipitation were also performed by FactSage for comparison. The leaching concentrations of hexavalent chromium were evaluated according to US-EPA-3060A method. The following conclusions could be drawn:

1. The main crystalline phases in slags with different amount of $B_2O_3$ addition were observed to be $Ca_2SiO_4$, merwinite, spinel, and akermanite.
2. 2% $B_2O_3$ addition is sufficient to eliminate the disintegration of synthetic slag by suppressing the phase transition to $\gamma$-$Ca_2SiO_4$.
3. The precipitation of $Ca_2SiO_4$ phase was suppressed by adding $B_2O_3$; however, excess $B_2O_3$ addition (> 2%) would significantly increase chromium concentration in $Ca_2SiO_4$ phase and overall chromium distribution in $Ca_2SiO_4$ phase.
4. Chromium was found to be enriched in spinel phase. The size of spinel phase increases with increasing $B_2O_3$ content in slag.
5. The hexavalent chromium leachability of slag was significantly enhanced with addition of $B_2O_3$ higher than 2%, which could be attributed to the enhanced chromium distribution in $Ca_2SiO_4$ phase. Therefore, excess boron oxide content (> 2%) should be avoided for stabilizing stainless steel slag.

**Acknowledgements** Open access funding provided byUniversity of Oulu including Oulu University Hospital. This work was supported by the Academy of Finland for Genome of Steel Grant (No. 311934) and Natural Science Foundation of China (NSFC Contract No. 51774026).

## References

1. Pillay K, Von Blottnitz H, Petersen J (2003) Ageing of chromium (III)-bearing slag and its relation to the atmospheric oxidation of solid chromium (III)-oxide in the presence of calcium oxide. Chemosphere 52:1771–1779. https://doi.org/10.1016/S0045-6535(03)00453-3
2. Tossavainen M, Engstrom F, Yang Q, Menad N, Larsson Lidstrom M, Bjorkman B (2007) Characteristics of steel slag under different cooling conditions. Waste Manag 27:1335–1344. https://doi.org/10.1016/j.wasman.2006.08.002
3. Chan CJ, Kriven WM, Young JF (1992) Physical stabilization of the β→γ transformation in dicalcium silicate. J Am Ceram Soc 75:1621–1627. https://doi.org/10.1111/j.1151-2916.1992.tb04234.x
4. Eriksson J, Björkman B (2004) MgO modification of slag from stainless steelmaking. In VII International Conference on Molten Slags, Fluxes and Salts, Cape Town, South Africa.
5. García-Ramos E, Romero-Serrano A, Zeifert B, Flores-Sánchez H-López M, Palacios EG (2008) Immobilization of chromium in slags using MgO and $Al_2O_3$. Steel Res Int 79:332–339. https://doi.org/10.1002/srin.200806135
6. Cabrera-Real H, Romero-Serrano A, Zeifert B, Hernandez-Ramirez A, Hallen-López M, Cruz-Ramirez A (2012) Effect of MgO and CaO/$SiO_2$ on the immobilization of chromium in synthetic slags. J Mater Cycles Waste Manag 14:317–324. https://doi.org/10.1007/s10163-012-0072-y
7. Cao LH, Liu CJ, Zhao Q, Jiang MF (2017) Effect of $Al_2O_3$ modification on enrichment and stabilization of chromium in stainless steel slag. J Iron Steel Res Int 24:258–265. https://doi.org/10.1016/S1006-706X(17)30038-9
8. Shu QF, Luo QY, Wang LJ, Chou K (2015) Effects of MnO and CaO/$SiO_2$ mass ratio on phase formations of CaO-$Al_2O_3$-MgO-$SiO_2$-$CrO_x$ slag at 1673 K and $P_{O2}=10^{-10}$ atm. Steel Res Int 86:391–399. https://doi.org/10.1002/srin.201400117
9. Li JL, Xu AJ, He DF, Yang QX, Tian NY (2013) Effect of FeO on the formation of spinel phases and chromium distribution in the CaO-$SiO_2$-MgO-$Al_2O_3$-$Cr_2O_3$ system. Int J Miner Metall Mater 20:253–258. https://doi.org/10.1007/s12613-013-0720-9
10. Albertsson GJ, Teng LD, Björkman B (2014) Effect of basicity on chromium partition in CaO-MgO-$SiO_2$-$Cr_2O_3$ synthetic slag at 1873 K. Miner Process Extract Metall 123:116–122. https://doi.org/10.1179/1743285513Y.0000000038
11. Albertsson GJ, Teng LD, Engström F, Seetharaman S (2013) Effect of the heat treatment on the chromium partition in CaO-MgO-$SiO_2$-$Cr_2O_3$ synthetic slags. Metall Mater Trans B 44:1586–1597. https://doi.org/10.1007/s11663-013-9939-0
12. Ghose A, Chopra S, Young JF (1983) Microstructural characterization of doped dicalcium silicate polymorphs. J Mater Sci 18:2905–2914. https://doi.org/10.1007/BF00700771
13. Seki A, Aso Y, Okubo M, Sudo F, Ishizaka K (1986) Development of a dusting prevention stabilizer for stainless steel slag. Kawasaki Steel Tech Rep 15:16–21
14. Durinck D, Arnout S, Mertens G, Boydens E, Tom Jones P, Elsen J, Blanpain B, Wollants P (2008) Borate distribution in stabilized stainless-steel slag. J Am Ceram Soc 91:548–554. https://doi.org/10.1111/j.1551-2916.2007.02147.x
15. Wu XR, Zhong QB, Shen XM, Cao FB, Wang P, Li LS (2018) Influence of $B_2O_3$ on crystallization behavior of Cr-bearing phase in stainless steel slag. In 2018 4th International Conference on Green Materials and Environmental Engineering, Beijing, China.
16. Shanxi Taigang Stainless Steel Co., Ltd (TISCO). A treatment method of stainless steel slag. Chinese Patent, CN 102586517 A (**in Chinese**)
17. Li WL, Xue XX (2018) Effects of boron oxide addition on chromium distribution and emission of hexavalent chromium in stainless-steel slag. Ind Eng Chem Res 57:4731–4742. https://doi.org/10.1021/acs.iecr.8b00499
18. U.S. EPA. United States Environmental Protection Agency. SW-846 Method 3060A. Test methods for evaluating solid wastes, Physical/Chemical Methods, SW-846 On Line, Rev.1, 1996. https://www.epa.gov/sites/production/files/2015-12/documents/3060a.pdf
19. Sevim F, Demir F, Bilen M, Okur H (2006) Kinetic analysis of thermal decomposition of boric acid from thermogravimetric data. Korean J Chem Eng 23:736–740. https://doi.org/10.1007/BF02705920
20. Shu QF, Li PF, Zhang X, Chou K (2016) Thermodynamics and structure of CaO-$Al_2O_3$-3 Mass Pct $B_2O_3$ slag at 1773 K (1500°C). Metall Mater Trans B 47:3527–3532. https://doi.org/10.1007/s11663-016-0781-z
21. Alexander L, Klug HP (1948) Basic aspects of X-ray absorption in quantitative diffraction analysis of powder mixtures. Anal Chem 20:886–889. https://doi.org/10.1021/ac60022a002
22. Bale CW, Chartrand P, Degterov SA, Eriksson G, Hack K, Ben Mahfoud R, Melançon J, Pelton AD, Petersen S (2002) FactSage thermochemical software and databases. Calphad 26:189–228. https://doi.org/10.1016/S0364-5916(02)00035-4
23. Durinck D, Tom Jones P, Blanpain B, Wollants P, Mertens G, Elsen J (2007) Slag solidification modeling using the Scheil-Gulliver assumptions. J Am Ceram Soc 90:1177–1185. https://doi.org/10.1111/j.1551-2916.2007.01597.x
24. Barbier J, Hyde BG (1985) The structures of the polymorphs of dicalcium silicate, $Ca_2SiO_4$. Acta Crystallogr Sect B 41:383–390. https://doi.org/10.1107/S0108768185002348
25. Pretorius BE, Snellgrove R, Muan A (1992) Oxidation state of chromium in CaO-$Al_2O_3$-$CrO_x$-$SiO_2$ melts under strongly reducing conditions at 1500°C. J Am Ceram Soc 75:1378–1381. https://doi.org/10.1111/j.1151-2916.1992.tb04197.x
26. Wang LJ, Seetharaman S (2010) Experimental studies on the oxidation states of chromium oxides in slag systems. Metall Mater Trans B 41:946–954. https://doi.org/10.1007/s11663-010-9383-3
27. De Villiers JPR, Muan A (1992) Liquidus-solidus phase relations in the system CaO-CrO-$Cr_2O_3$-$SiO_2$. J Am Ceram Soc 75:1333–1341. https://doi.org/10.1111/j.1151-2916.1992.tb04191.x
28. Cuesta A, Losilla RE, Aranda AGM, Sanz J, De la Torre GÁ (2012) Reactive belite stabilization mechanisms by boron-bearing dopants. Cem Concr Res 42:598–606. https://doi.org/10.1016/j.cemconres.2012.01.006
29. Cormier L, Ghaleb D, Delaye JM, Calas G (2000) Competition for charge compensation in borosilicate glasses: Wide-angle x-ray scattering and molecular dynamics calculations. Phys Rev B 61:14495. https://doi.org/10.1103/PhysRevB.61.14495
30. Voorhees PW (1985) The theory of Ostwald ripening. J Stat Phys 38:231–252. https://doi.org/10.1007/BF01017860

31. Baldan A (2002) Review progress in Ostwald ripening theories and their applications to nickel-base superalloys Part I: Ostwald ripening theories. J Mater Sci 37:2171–2202. https://doi.org/10.1023/A:1015388912729
32. Edward JT (1970) Molecular volumes and the Stokes-Einstein equation. J Chem Educ 47:261. https://doi.org/10.1021/ed047p261
33. Li QH, Yang SF, Zhang YL, An ZQ, Guo ZC (2017) Effects of MgO, $Na_2O$, and $B_2O_3$ on the viscosity and structure of $Cr_2O_3$-bearing CaO-$SiO_2$-$Al_2O_3$ slags. ISIJ Int 57:689–696. https://doi.org/10.2355/isijinternational.ISIJINT-2016-569
34. EC Decision 2003/33/EC. Council Decision of 19 December 2002 establishing criteria and procedures for the acceptance of waste at landfills pursuant to Article 16 of and Annex II to Directive 1999/31/EC. Official Journal L 011, 16/01/2003, p.0027–0049.
35. Engström F, Adolfsson D, Samuelsson C, Sandström Å, Björkman B (2013) A study of the solubility of pure slag minerals. Miner Eng 41:46–52. https://doi.org/10.1016/j.mineng.2012.10.004
36. Strandkvist I, Björkman B, Engström F (2015) Synthesis and dissolution of slag minerals-a study of β-dicalcium silicate, pseudowollastonite and monticellite. Can Metall Quart 54:446–454. https://doi.org/10.1179/1879139515Y.0000000022
37. Teratoko T, Maruoka N, Shibata H, Kitamura S (2012) Dissolution behavior of dicalcium silicate and tricalcium phosphate solid solution and other phases of steelmaking slag in an aqueous solution. High Temp Mater Proc 31:329–338. https://doi.org/10.1515/htmp-2012-0032
38. Samada Y, Miki T, Hino M (2011) Prevention of chromium elution from stainless steel slag into seawater. ISIJ Int 51:728–732. https://doi.org/10.2355/isijinternational.51.728